ACCSCIENCE PUBLISHING

Advances in Radiotherapy & Nuclear Medicine

ORIGINAL RESEARCH ARTICLE

Impact of beam pulse structure on yield of reactive oxygen species during proton FLASH radiotherapy

Jonathan Phillips[1,2] and Giuseppe Schettino[1]*

[1]Department of Medicine, Marine, and Nuclear, National Physical Laboratory, London, United Kingdom

[2]Department of Physics, School of Mathematics and Physics, Faculty of Engineering and Physical Sciences, University of Surrey, Guildford, United Kingdom

Abstract

This study investigates the yield of reactive oxygen species (ROS) under proton FLASH irradiation in well-oxygenated healthy tissue to identify the beam time structure for the lowest ROS yield. Examining the influence of proton beam time structure on radiolytic oxygen consumption and ROS production directly addresses the oxygen depletion hypothesis for the FLASH effect. A bespoke Monte Carlo Geant4-DNA model was used to simulate water radiolysis under a proton FLASH dose rate and output time-resolved G values for the principal radiolysis products. A 1.6 µm cube of water with fixed oxygen concentration was modelled for pulse lengths and periods ranging from 1 ns to 1 ms and 10 ns to 10 ms, respectively. The study was limited to two ROS species (hydroxyl radical [$OH^{\cdot}$] and hydrogen peroxide [H_2O_2]) and a pulse-structure grid for which the pulse period was constrained to be 10 times the pulse length. The maximum and total G values, G_{max} and G_{tot}, were used to determine the beam time structure that produced the fewest $OH^{\cdot}$ and H_2O_2. The model shows that the pulse period affected the yield of ROS more than the pulse length. This indicates that the yield of the investigated ROS decreases most under short pulse periods combined with the longest possible pulse duration within those periods. The method of high dose rate proton delivery that is closest to these parameters is an isochronous cyclotron emitting 2 ns pulses separated by 13.7 ns. However, this study also suggests that the oxygen depletion hypothesis cannot fully explain the FLASH effect, as the yield of $OH^{\cdot}$ in healthy tissue is higher for FLASH irradiation than for conventional irradiation. These conclusions should be interpreted within the limitations of the model, which assumes static oxygenation in a single microscopic volume and explores a restricted set of pulse structures and ROS species. Further work is therefore required to assess the generality of these findings under more realistic biological conditions.

Keywords: FLASH radiotherapy; Proton; Geant4-DNA; Simulation; Reactive oxygen species; Pulse structure

***Corresponding author:**
Giuseppe Schettino
(giuseppe.schettino@npl.co.uk)

Citation: Phillips J, Schettino G. Impact of beam pulse structure on yield of reactive oxygen species during proton FLASH radiotherapy. *Adv Radiother Nucl Med*. 2026;4(3):026180016. doi: 10.36922/ARNM026180016

Received: April 30, 2026

Revised: July 14, 2026

Accepted: July 24, 2026

Published online: August 19, 2026

Copyright: © 2026 Author(s). This is an Open-Access article distributed under the terms of the Creative Commons Attribution License, permitting distribution, and reproduction in any medium, provided the original work is properly cited.

Publisher's Note: AccScience Publishing remains neutral with regard to jurisdictional claims in published maps and institutional affiliations.

1. Introduction

1.1. Differences between conventional and FLASH radiotherapy

The main advantage proposed for FLASH radiotherapy is the preferential sparing of healthy tissue relative to tumour tissue, known as the FLASH effect. This effect would significantly decrease the probability of side effects experienced by patients when compared to conventional radiotherapy. This sparing is therefore expected to enable treatment optimisation by permitting dose escalation to the tumour or improved treatment conformality.[1]

Current clinical conventional radiotherapy treatments require 1–10 minute exposures daily, over 5 to 8 weeks, with a dose rate of around 0.1 Gy/s.[2,3] The fractionation of these exposures is meant to allow the patient's healthy tissue to recover from the ionising radiation so that the overall side effects experienced by the patient are minimised.[4] In contrast, a FLASH radiotherapy treatment would offer 100 ms daily irradiations,[3] over one week, with a dose rate above 40 Gy/s.[2,5-11] This drastic decrease in treatment time is an additional advantage of FLASH radiotherapy, as ultra-short irradiations may also improve patient comfort and treatment tolerability while increasing clinical throughput and reducing burns on healthcare providers.

1.2. Hypotheses for the FLASH effect

Despite many studies on FLASH radiotherapy, the mechanisms underpinning the FLASH effect are still unknown.[5,8] There are multiple hypotheses to explain the FLASH effect's occurrence, including the oxygen depletion hypothesis, the DNA damage hypothesis, and the immunoreaction hypothesis.[12]

The DNA damage hypothesis explains the sparing of healthy tissue through different repair pathways between conventional and FLASH irradiations, as the spatio-temporally highly dense clustered damage produced by FLASH may be processed differently by tumour and healthy cellular repair mechanisms. Specifically, normal cells have intact cell cycle checkpoints and high-fidelity DNA repair pathways, enabling more effective processing of the complex clustered lesions produced by FLASH irradiation, whereas cancer cells often exhibit defective damage sensing and repair and are therefore less able to resolve such spatially and temporally concentrated damage.

The immunoreaction hypothesis proposes that incident radiation changes the immunological response to radiation in healthy tissue. Tumours possess a chronically immunosuppressed microenvironment with abnormal signalling pathways and reduced capacity to mount rapid immune responses. This means that the dose-rate differences between FLASH and conventional irradiations may have a larger impact on the immune activity of healthy tissue. Hence, FLASH would spare healthy tissue but would not reduce the effectiveness of tumour control.

While the other hypotheses are strong contenders to explain the FLASH effect, this study focuses on the oxygen depletion hypothesis. It relies on the rapid depletion of cellular oxygen through the radiolysis of cellular water under an ultra-high dose rate (UHDR) beam. The depletion of cellular oxygen would lead to fewer reactive oxygen species (ROS) being produced in healthy cells. Therefore, the radioresistance of healthy cells would increase compared to that of cancer tissue. ROS contribute approximately 70% of the radiation-induced DNA damage in healthy cells and, because their production through water radiolysis occurs on time scales relevant to FLASH irradiation, they are a key candidate mechanism for the FLASH effect. A diagram highlighting the complexity and the timescale of water radiolysis is shown in Figure 1. As cancer tissue is naturally hypoxic, the difference in oxygen concentration in the tumour before and after the FLASH irradiation would be negligible; hence, the FLASH effect would not affect tumour tissue as much.[1,13]

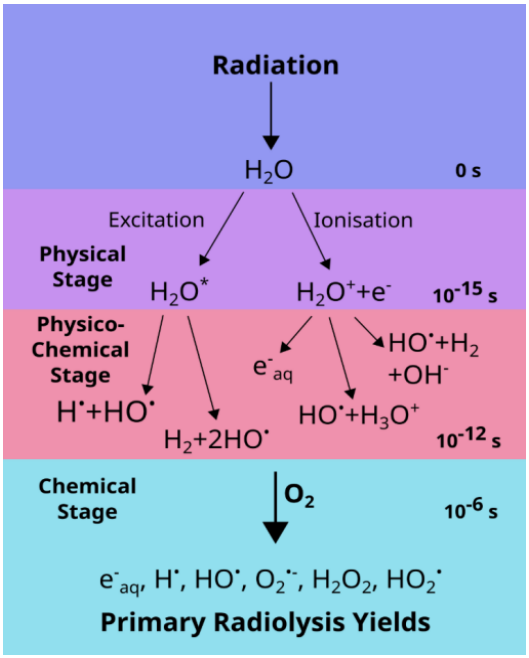

Figure 1. Stages of water radiolysis with processes and products of each stage. Oxygen molecules enable the final, chemical stage (light blue) reactions to produce reactive oxygen species around the microsecond (10^{-6} s) mark. Adapted from Sartorio *et al.*[14]

While the actual effect of oxygen depletion during FLASH radiotherapy remains debated amidst the other

hypotheses, it is one of the leading models for the FLASH effect.[15-17] This is due to it providing a direct reasoning for the healthy tissue sparing through its increased radioresistance compared to cancer tissue, which is hypoxic by nature. This is reinforced by experimental data on radiation damage in the presence and absence of oxygen.[17] Even if oxygen depletion is not the sole mechanism behind the FLASH effect, it is likely that the temporal characteristics of FLASH irradiation alter the radiation chemistry stage of the radiobiology pathway. The extremely high instantaneous dose rate increases the probability that radicals produced by separate radiation tracks interact within the same chemical stage event, which does not occur under conventional dose rates. This can lead to reduced concentrations of damaging species in healthy tissue under FLASH dose rates.

1.3. Monte Carlo simulations: Geant4

In this study, the Geant4 toolkit for Monte Carlo track-structure simulations was used to model the radiolysis of water under proton FLASH irradiation. To simulate this process, the Geant4-DNA extension was needed to simulate the chemical reactions necessary for water radiolysis.[18-22] The model was split into two separate simulation phases. The first phase models the physical stage of radiolysis, where water molecules are excited and/or ionised, leading to the formation of primary radicals and molecular species, and the second phase models the chemical stage, where these primary species diffuse and interact through radical–radical and radical–molecule reactions to form secondary radicals that are tracked and quantified. The model setup is explained in more detail in **Section 2**.

1.4. Aims and objectives

This study's main aim was to investigate the yield of ROS under a proton FLASH radiotherapy beam, and assess the difference in ROS yield as a function of the beam pulse structure.

The model was initially validated through a comparison with published data. Its results for an electron FLASH irradiation were compared to those published by Chappuis *et al.*[23] This study was selected for verification because their Geant4-DNA simulations were directly benchmarked against experimental measurements of water radiolysis under UHDR electron irradiation. This provides a reliable reference point for validating our model against results that have already been compared with experimental data. Once the model was verified, the beam type was changed to protons, and the time structure was varied to obtain the results presented in **Section 3**.

While FLASH radiotherapy studies have traditionally focused on the role of the average dose rate, far less is known about the impact of the beam time structure, even when the same average dose rate is delivered.[24-26] This motivates the present study, which investigates the influence of pulse structure on ROS yield using a two-phase Monte Carlo approach that explicitly models both the physical and chemical stages of radiolysis, thereby providing new insight into oxygen depletion mechanisms underlying the FLASH effect. To cover a wide range of values, the pulse lengths and periods vary logarithmically from 1 ns to 1 ms and 10 ns to 10 ms, respectively; the ROS species, hydroxyl radical ($OH^{\bullet}$) and hydrogen peroxide (H_2O_2); and a statically oxygenated, 1.6-μm cube of water were used to model cellular material under FLASH irradiation.

This study focuses on $OH^{\bullet}$ and H_2O_2 because they represent two of the most biologically relevant products of water radiolysis. $OH^{\bullet}$ is the most chemically reactive ROS and a major contributor to radiation-induced indirect DNA damage, while H_2O_2 is a longer-lived molecular oxidant that can diffuse farther from the initial radiation track. Together, they provide complementary information. The remaining radiolysis products generated by Geant4-DNA were not analysed in detail to limit the parameter space.

2. Materials and methods

2.1. Simulations

2.1.1. Physical stage

The first part of the model was dedicated to measuring the energy distribution of the proton beam at different depths inside a water tank of side length 40 cm. The setup is shown schematically in Figure 2 along with the integral depth dose (IDD) curve for a 250 MeV proton beam travelling through water.

This model assumed a mono-energetic beam of protons. Although this is not a realistic proton beam as it does not account for the energy spread of a typical clinical beam, it is a reasonable assumption as clinical scenarios can be reconstructed by appropriately weighting different mono-energetic beams, and the setting took into account the proton interactions with water, which led to specific energy distributions at specific depths. Furthermore, a mono-energetic beam provides a controlled way to compare the proton energy distributions at different depths in the water tank.

This beam was constructed using the Geant4 General Particle Source tool, which allows the user to define the energy and the spatial and angular distributions of the beam. Here, the beam was set to a 1 mm circular and plane beam spot of 250 MeV protons.

The proton energy distributions were calculated at two

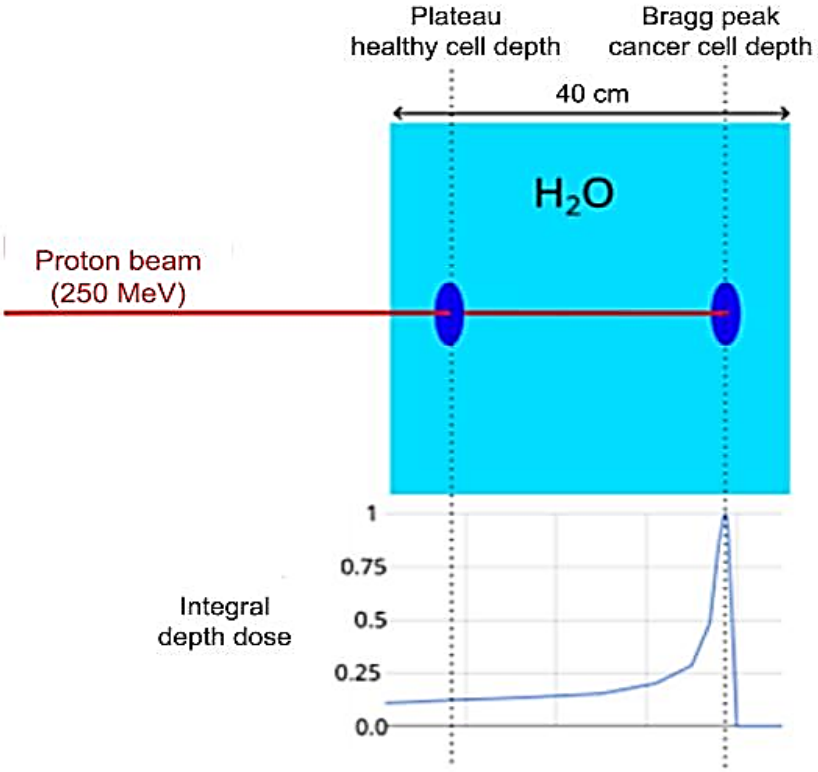

Figure 2. Sketch of the physical stage simulation showing its geometry and the points at which the proton energy is measured for the plateau region and the Bragg peak region of the proton integral depth dose curve for a 250 MeV proton beam travelling through water. These regions correspond to the placement of healthy and cancer tissue, respectively. This figure is original content.

depths: one near the entrance of the water tank around the plateau region of the IDD, and one deeper in the water tank at the Bragg peak's location. These two depths were chosen as they correspond to the depths of healthy tissue and cancer tissue, respectively, inside a patient's body. The focus of this study was to research the effects of time structure on the ROS yield in healthy tissue. Therefore, the energy distribution at the plateau of the IDD was used for most of the results presented in **Section 3**, but some tests on the ROS yield in cancer tissue are also presented in **Section 3.2** to show the difference between the tissue types.

2.1.2. Chemical stage

The second simulation phase modelled the chemical stage of the radiolysis process to estimate the amount of ROS produced for the time structure used in the proton beam simulation. It was based on an adapted version of a model published with the Geant4 version 11.4.0 beta release.[27] This beta release was later incorporated into a full release in Geant4 version 11.4.0, with the finalised version of the example used here.[28]

The published code simulated water radiolysis in a small cube of water by introducing primary particles at random times within the user-defined time structure. Through the independent reaction times method,[29] it resolved each reaction induced by the primary and secondary particles in order of shortest reaction time until all reactions were resolved, and then output the time-resolved G value curves for each of the ROS of interest. The G value measures how many particles of a specific species are formed per 100 eV of radiation energy absorbed.[30] These values were used to link the G value to cell damage because ROS directly damage a cell's DNA, with the hydroxyl radical $OH^{\bullet}$ being the most toxic ROS in biological systems. The underlying radiolysis chemistry model was identical to that used by Chappuis *et al.*[23], which itself was benchmarked against experimental measurements of water radiolysis under UHDR electron irradiation. The model employed the standard Geant4-DNA chemistry framework and reaction network implemented in Geant4 version 11.4, including the diffusion and reactions of the principal radiolytic species generated during water radiolysis. No modifications were made to the reaction scheme, reaction rate constants, or

transport parameters. The present work therefore focuses on the influence of radiation type and beam time structure, while retaining the radiolysis parameters validated by Chappuis *et al.*[23] as the reference chemistry model.

To recreate the results presented by Chappuis *et al.*[23], the parameters used in this study mimicked theirs. Therefore, the first change was to change the physics list parameter from the default G4EmDNAPhysics_option2 to G4EmDNAPhysics_option4. As discussed by Chappuis *et al.*[23], option 2 can only model electron interactions in water up to 1 MeV, and the results to be recreated use an electron beam with an energy of 5–6 MeV. Option 4 is capable of modelling electron interactions up to electron energies of 10 MeV, so this was used in all simulations in this study, as this comfortably encompasses the full energy range of secondary electrons produced by 250 MeV protons in water, which are predominantly in the eV–keV range with only a sparse high-energy tail.

Furthermore, the initial example code used a single energy for the primary particles entering the small cube of water, so an energy distribution was incorporated into the primary generator's energy. As in **Section 2.1.1**, the primary particle source was created using the Geant4 General Particle Source tool, and the spectral distribution of the primary electrons/protons was set to a Gaussian distribution taken from the simulation of the physical stage. Here, the primary particles were set to begin their tracks at random locations on one side of the cube, i.e., with a square and plane "beam spot."

In contrast to Chappuis *et al.*[23]'s work, this model did not rely on a separate differential equation solver, but rather modelled the diffusion of particles in Geant4-DNA itself between each of the modelled pulses.

This section of the model shows the evolution of ROS yield with time in a 1.6-μm cube of water. The size of this cube was chosen to be sufficiently large to accommodate many reactions between the incident protons and water molecules, but not so large that it drastically increases the computing time of the model. This volume is also biologically relevant, as it is comparable to the size of intracellular compartments. It is also the size used in the study used for benchmarking the simulation model developed within this work. Furthermore, the choice of a 1.6-μm cube was physically motivated by the spatial and temporal scales of water radiolysis. The highly reactive radical species investigated here, particularly $OH^{\bullet}$, have lifetimes of the order of nanoseconds and diffusion ranges typically limited to tens of nanometres before reacting. Consequently, the radical–radical interactions that were hypothesised to contribute to the FLASH effect occurred predominantly within a highly localised volume surrounding the radiation tracks. Extending the simulation geometry to dimensions comparable to or larger than a whole cell would therefore introduce regions where radicals have a negligible probability of interacting with one another before being consumed. The selected volume was sufficiently large to contain many overlapping proton tracks and their associated chemical species while remaining focused on the local interaction processes that govern FLASH-induced changes in ROS yield and composition. To further model the difference between healthy and cancer tissue, an oxygen partial pressure was set for each type of cell: 21% for healthy tissue, and 0.7% for cancer tissue. Here, the percentage partial pressure corresponds to the ratio of the number of molecules of oxygen O_2 in the cube to the total number of molecules in the cube. These values were chosen because cell culture experiments are generally performed at atmospheric partial pressure for O_2 (21%), and the partial pressure of hypoxic cancer tissue is less than 1%,[31] so an arbitrary factor of 30 between the oxygen levels of these tissues was used for this project; hence, the value of 0.7% in cancer cells. Then, a time signature was assigned to each proton introduced into the system to mimic the pulse structure of a radiotherapy beam and thereby define the pulse length (width of a single pulse), period (time between the beginning of two consecutive pulses), and thus the average dose rate. The simulation continually introduced primary particles until the user-defined total dose was reached in the cube of water. This lets the user indirectly define the average dose rate R (set to 40 Gy/s in this study) as **Equation 1**:

$$R = \frac{D}{NT} \tag{1}$$

where D is the total dose, N is the number of beam pulses simulated, and T is the period of each of those pulses. D, N, and T are variables that were set within the macro file of the model, and this simulation then constructed plots of G value against time throughout the irradiation. This average dose rate R is not to be confused with the instantaneous dose rate inside the pulse, which is higher than the average dose rate.[32] For example, if we take R = 40 Gy/s, D = 20 Gy, with 1 ns pulses (pulse length) every 10 ns (pulse period T), then the instantaneous dose rate within each of the 50 million pulses (number of pulses N) is 400 Gy/s.

The primary particles here were assigned time signatures which were randomly distributed according to the time structure defined by the period and pulse length. Primary particles were then introduced until the total cut-off dose was reached, at which point the time-structured evolution of chemical reactions was simulated to form the ROS studied, using the time signature of each

primary particle in the model. This means that there is no set number of primary particles to be introduced into the system, as the exact number would be linked to the random interactions between the particles and the surrounding medium (water).

To ensure reproducibility, seeds 1–1,000 were used to estimate the G values presented in **Section 3**. Geant4 produced a unique array of reproducible values from the initial user-defined seeds, which were then cascaded down to the threads. Furthermore, the oxygenated water was irradiated for 0.5 seconds (D = 20 Gy at R = 40 Gy/s) in the FLASH case and 200 seconds (D = 20 Gy at R = 0.1 Gy/s) in the conventional case, and the model simulated the diffusion of ROS up to 300 seconds after the beginning of the irradiation in both cases. Finally, Geant4 required a minimum distance for each step of the simulation; this cut was set to 0.01 mm, and a minimum production energy for secondary particles; this cut was set to 100 eV. These cuts ensure that the model runs smoothly and reasonably quickly.

2.2. Total and maximum G values

Once the plots of G value against time were output from the second simulation, the data must be described through some parameter so that the yields for different time structures can be compared to find the time structure with the lowest ROS yield. For this purpose, the maximum and total G values, G_{max} and G_{tot}, respectively, were taken from each of the output plots and compared. G_{tot} was calculated by integrating the G value curve to describe its overall evolution for different pulse structures, while G_{max} describes the instantaneous evolution of the G value throughout the irradiation. Using both parameters provides a way to test similarities and differences between instantaneous and overall evolution, and should indicate how reliable the results are through similarities in trends.

2.3. Variables and fixed parameters

To investigate the beam time structure which yielded the fewest ROS, this study focused on varying the temporal parameters: the pulse period T and the pulse length L. It was assumed here that all other parameters remain fixed at the values defined in Table 1. Because the average dose rate remained constant, the number of pulses N referenced in **Equation 1** also varied according to the pulse period T.

The values of the fixed parameters are common in radiobiology studies, with a proton beam energy of 250 MeV, a cut-off dose of 20 Gy, and oxygen partial pressures in healthy and cancer tissue of 21% and 0.7%. A total cut-off dose of 20 Gy was chosen because single-fraction doses in the 10–30 Gy range have been reported in preclinical FLASH studies[33-35] and similar dose levels are deemed to be required to produce measurable oxygen depletion and radical–radical interaction effects during the early radiation chemistry stage.[15,17] As for the dose rate, it was set to 40 Gy/s as this is generally accepted as the threshold dose rate above which the FLASH effect is observed.[2,5-11] The pulse length and period varied between 1 ns and 1 ms, and 10 ns and 10 ms, respectively. A logarithmic sampling of the parameters was used to span a wide range of values while limiting the total number of simulations required.

Table 1. Each parameter used in the model with its range of values

Parameter	Variable/Constant	Range/Value
Beam energy	Constant	250 MeV
Pulse length L	Variable	1 ns–1 ms
Pulse period T	Variable	10 ns–10 ms
Radiation type	Constant	Protons
Total cut-off dose	Constant	20 Gy
Average dose rate for FLASH	Constant	40 Gy/s
Healthy tissue oxygen partial pressure	Constant	21%
Cancer tissue oxygen partial pressure	Constant	0.7%

3. Results and discussion

3.1. Verification of model through electron irradiation

As mentioned in **Section 1.4**, the first step of this study was to verify that the model used was reliable and accurate to reality. For this purpose, an electron FLASH irradiation was modelled and compared to the results presented by Chappuis *et al.*[23] The parameters used in this step are given in Table 2. The results produced here are compared to those published by Chappuis *et al.*[23] in Figure 3.

Table 2. Values used for each relevant parameter in the reproduction of Chappuis *et al.*[23] results

Parameter	Value
Radiation type	Electron
Beam energy	6 MeV
Pulse length	1.8 μs
Number of pulses	1
Cut-off dose	1 Gy
Oxygen concentration	21%

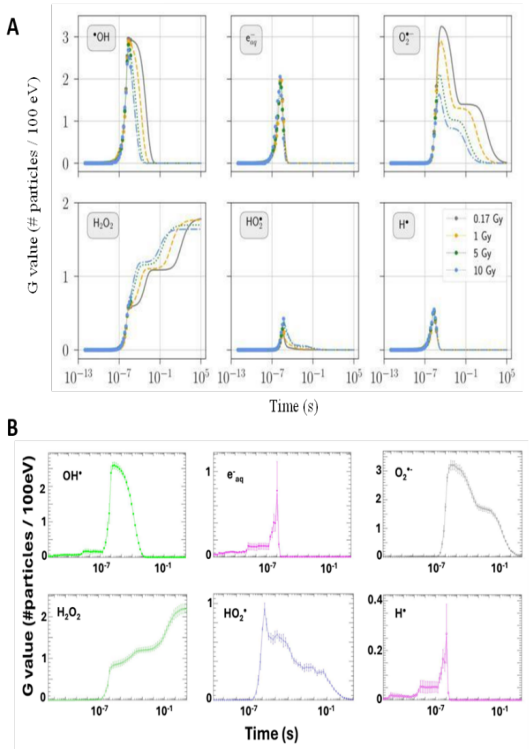

Figure 3. Comparison of published results and the model developed in this study as verification. Plots show G value against time for the six main products of radiolysis: OH•, e^-_{aq}, $O_2^{\bullet-}$, H_2O_2, $HO_2^{\bullet}$, and H•. (A) Results adapted from Chappuis *et al.*[23] (B) Results from this study.

From Figure 3, it is clear that the results of the two models are very similar. The trends in ROS G value are the same, with the peaks in production at the same time in both models: around 10^{-6} seconds. Taking the example of the plots of the OH• production, the peak in production began around 10^{-7} seconds and reached its maximum value around 10^{-6} seconds. This is the same for both Chappuis *et al.*[23]'s results and those presented here.

However, there is a small difference in scale for the e^-_{aq} and the $HO_2^{\bullet}$ radicals. For e^-_{aq}, the maximum G value achieved is around 2 particles/100 eV for Chappuis *et al.*[23]'s results, and around 1 particle/100 eV for the results presented in this study. Furthermore, for $HO_2^{\bullet}$, the maximum G value achieved is around 0.5 particles/100 eV in Chappuis *et al.*[23], and around 1 particle/100 eV in this study. Such small discrepancies are expected, as the yields of e^-_{aq} and $HO_2^{\bullet}$ are particularly sensitive to details of the chemical stage modelling (which differ between the two studies) and are small enough to be consistent with the statistical uncertainties of the Monte Carlo simulations (although uncertainties are not reported in the work of Chappuis *et al.*[23]). The fact that the plots are similar shows that the models produced close to the same results and therefore the model can be used for the rest of the study without further changes.

3.2. Comparison of conventional radiotherapy against FLASH, and healthy tissue against cancer tissue

Next, to show that the FLASH effect is caused by the yield of ROS, the yields were compared for FLASH and conventional irradiations, in both healthy and cancer tissue. Here, only the yield of the OH• was used as it is the most reactive and toxic ROS in biological systems.[36-38] All uncertainties reported here are statistical uncertainties, scaling with $\sqrt{N}$, where N is the number of events simulated. These were taken directly from the Geant4 outputs.[39] The model presented in this study assumes no error in the initial beam energy of 250 MeV, as well as for the oxygen concentrations of 21% and 0.7% for healthy and cancer tissues, respectively.

In Figure 4, the yield of OH• in cancer tissue is similar for both FLASH and conventional irradiations. While the G values did not overlap with each other, both the maximum and total G values were within two standard deviations of each other, with approximately 2–3% uncertainty. This means that the values are overall close together, and if the FLASH effect is due to the oxygen depletion hypothesis, then FLASH radiotherapy does indeed maintain the same tumour control efficacy as conventional radiotherapy. Although the maximum and total G values remained similar between FLASH and conventional irradiation in the tumour simulations, the temporal evolution differed noticeably. In the FLASH case, the G value decreased more rapidly after reaching its peak because the radicals are produced within a shorter time window, increasing the probability of radical–radical interactions and recombination reactions. Under conventional irradiation, radical production was distributed over a longer timescale, leading to a more sustained balance between species generation and removal. As a result, the G value remained approximately constant for longer before eventually decreasing. This difference in temporal behaviour highlights the influence of beam time structure on chemical stage kinetics, even when the integrated radical yield remains largely unchanged.

However, for both G_{max} and G_{tot}, the conventional OH• yield in healthy tissue was only around 60% that of the FLASH exposure. This is contrary to expectations, as the oxygen depletion hypothesis suggests that the yield of ROS in healthy tissue should be lower for FLASH than it is for conventional radiotherapy. But despite the OH• yield in healthy tissue not being what was expected, there is still a large decrease in OH• production between cancer tissue and healthy tissue. This decrease was evident both in the

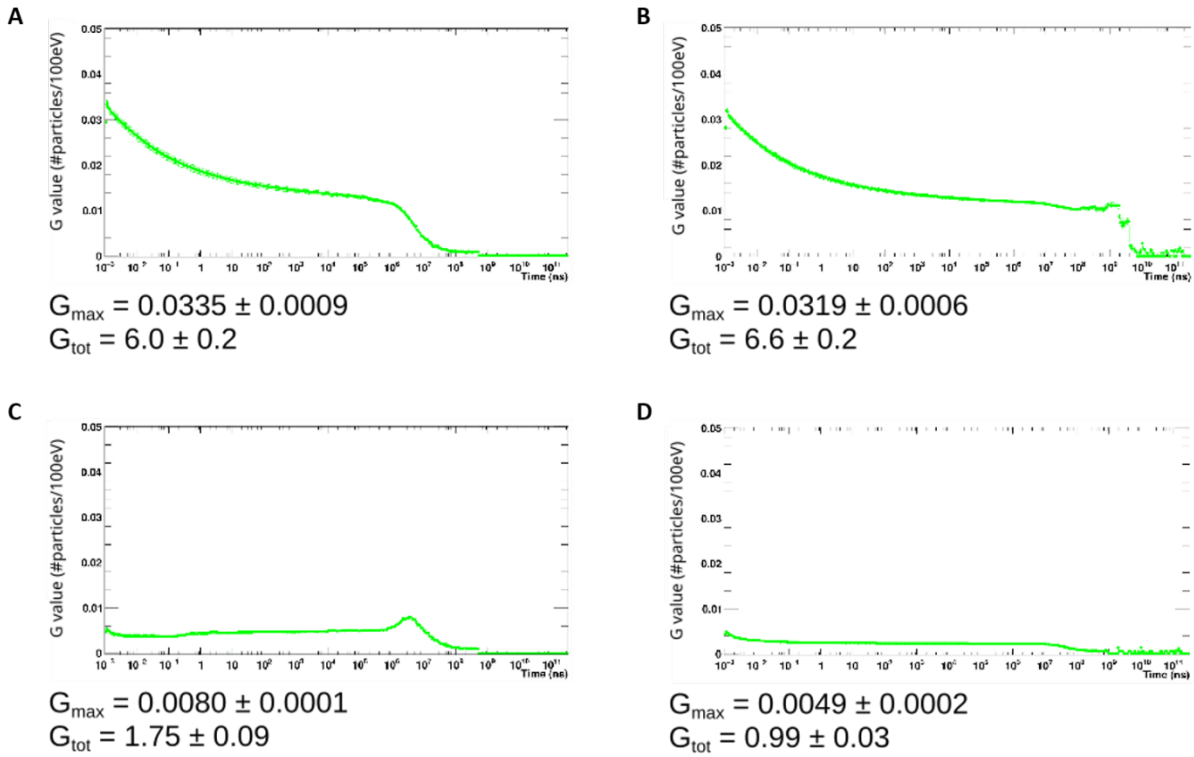

Figure 4. Comparison of the OH• yield between FLASH and conventional modalities, and between cancer tissue and healthy tissue. G_{max} and G_{tot} refer to the maximum and total G values, respectively, for each plot of G value against time. Each plot was set to have the same scale on the vertical axis to make the plots easier to compare visually. The G values shown here are in particles/100 eV. Cancer tissue (0.7% O_2; 25 ± 6 MeV) with (A) FLASH (40 Gy/s; 1 µs *L*; 10 µs *T*) and (B) conventional irradiation (0.1 Gy/s; 1 s *L*; 2 s *T*). Healthy tissue (21% O_2; 238.1 ± 6 MeV) with (C) FLASH (40 Gy/s; 1 µs *L*; 10 µs *T*) and (D) conventional irradiation (0.1 Gy/s; 1 s *L*; 2 s *T*). *L* refers to the pulse length, and *T* corresponds to the period of the pulse. The percentage shown is the partial pressure of oxygen molecules in the water cube, with a lower partial pressure in cancer tissue than in healthy tissue; the value in MeV corresponds to the energy of the protons input into the simulation.

values of G_{max} and G_{tot} for the two types of tissue, and in the significant decrease in scale of the G value plots.

3.3. Determinants of reactive oxygen species yield

When looking into the variation of ROS yield with time structure, this study focused on the OH•, with the same reasoning as in **Section 3.2**. These results were also compared to the yields of H_2O_2, as these were seen to have opposite trends after the initial rise in Figure 3. This was performed to compare multiple ROS and begin generalising the results presented here to a broader range of ROS rather than a single species.

In Figure 5, both G_{max} and G_{tot} are shown for each set of pulse length and period. These values ranged as described in Table 1. In these results, the colour gradient was chosen so that green corresponded to lower yields and red corresponded to higher yields. These results give a general indication of the trends in G value linked to each of the two varied parameters. Comparing the progression of G values along the 1 ns pulse length column and the 10 ms period row of these tables, represented in Figure 5 by arrows a and b, respectively, it is clear that the pulse period affected the yield more than the pulse length. In fact, for a set pulse length of 1 ns (arrow a), the G values increased by a factor of ~10 between pulse periods of 10 ns and 10 ms, whereas for a fixed pulse period of 10 ms (arrow b), the G values decreased by a factor of ~3 for G_{max} and ~6 for G_{tot}, between pulse lengths of 1 ns and 1 ms. Table 3 shows the values of G_{max} and G_{tot} at each of these points. This shows that to limit the yield of ROS, a FLASH radiotherapy beam would need a long pulse length and a short period, as the G values increased with increasing period and decreased with increasing pulse length. Consequently, the ideal time structure for the beam lies on the diagonal in Figure 5, represented by arrow c.

Therefore, the evolution of G values along arrow c was studied in greater detail for OH• and H_2O_2. Along this diagonal, the pulse period was constrained to be 10

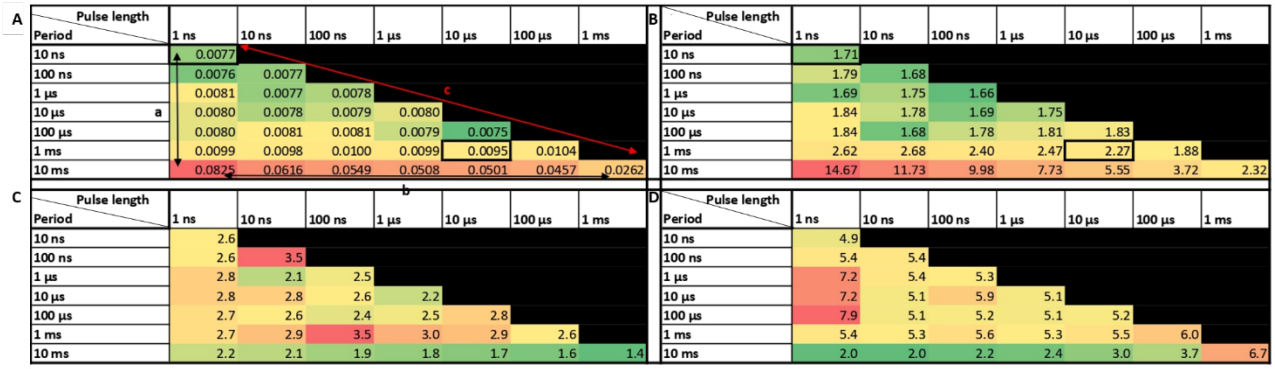

A

Period \ Pulse length	1 ns	10 ns	100 ns	1 µs	10 µs	100 µs	1 ms
10 ns	0.0077						
100 ns	0.0076	0.0077					
1 µs	0.0081	0.0077	0.0078				
10 µs	0.0080	0.0078	0.0079	0.0080			
100 µs	0.0080	0.0081	0.0081	0.0079	0.0075		
1 ms	0.0099	0.0098	0.0100	0.0099	0.0095	0.0104	
10 ms	0.0825	0.0616	0.0549	0.0508	0.0501	0.0457	0.0262

B

Period \ Pulse length	1 ns	10 ns	100 ns	1 µs	10 µs	100 µs	1 ms
10 ns	1.71						
100 ns	1.79	1.68					
1 µs	1.69	1.75	1.66				
10 µs	1.84	1.78	1.69	1.75			
100 µs	1.84	1.68	1.78	1.81	1.83		
1 ms	2.62	2.68	2.40	2.47	2.27	1.88	
10 ms	14.67	11.73	9.98	7.73	5.55	3.72	2.32

C

Period \ Pulse length	1 ns	10 ns	100 ns	1 µs	10 µs	100 µs	1 ms
10 ns	2.6						
100 ns	2.6	3.5					
1 µs	2.8	2.1	2.5				
10 µs	2.8	2.8	2.6	2.2			
100 µs	2.7	2.6	2.4	2.5	2.8		
1 ms	2.7	2.9	3.5	3.0	2.9	2.6	
10 ms	2.2	2.1	1.9	1.8	1.7	1.6	1.4

D

Period \ Pulse length	1 ns	10 ns	100 ns	1 µs	10 µs	100 µs	1 ms
10 ns	4.9						
100 ns	5.4	5.4					
1 µs	7.2	5.4	5.3				
10 µs	7.2	5.1	5.9	5.1			
100 µs	7.9	5.1	5.2	5.1	5.2		
1 ms	5.4	5.3	5.6	5.3	5.5	6.0	
10 ms	2.0	2.0	2.2	2.4	3.0	3.7	6.7

Figure 5. Values of G_{max} and G_{tot} in healthy tissue for varying pulse lengths and periods as a quantitative description of $OH^{\bullet}$ yield with percentage uncertainties shown in the corresponding cells. (A) Max OH G value (#particles/100 eV) and (C) corresponding percentage error (%). (B) Total OH G value (#particles/100 eV) and (D) corresponding percentage error (%). The colour gradient between the data points is set to be closer to green for lower values, and closer to red for higher values. For both G_{max} and G_{tot}, the two data points outlined in black are the G values for 1 ns pulse length, 10 ns period, and 10 µs pulse length, 1 ms period. These are highlighted as they correspond to the data with the closest time structures to those currently available with proton accelerators.[40]

times the pulse length (T = 10 L). The resulting trends are shown in Figure 6. For both species, G_{max} and G_{tot} varied approximately linearly with pulse length over the range investigated. Because T and L decreased simultaneously along this trajectory, the lowest ROS yields occurred at the shortest pulse lengths and pulse periods shown. This does not contradict the conclusion drawn from Figure 5 that the pulse period is the dominant parameter. When the two parameters were varied independently, reducing T lowered the ROS yield more strongly than increasing L. Consequently, the most favourable beam structure is one with the shortest achievable pulse period and the longest pulse length that can be accommodated within that period.

Table 3. G_{max} and G_{tot} values for each of the points of interest from Figure 5

Time structure (T=period; L=pulse length)	G_{max} (particles/100 eV)	G_{tot} (particles/100 eV)
T = 10 ns; L = 1 ns	0.0077	1.71
T = 10 ms; L = 1 ns	0.0825	14.67
T = 10 ms; L = 1 ms	0.0262	2.32

In Figure 5, the two data points outlined in black correspond to the closest time structures to those that current proton accelerators can achieve.[40] One of these points sits on the diagonal, which is plotted in Figure 6. Therefore, of the two types of UHDR proton beam delivery that are currently available with proton accelerators, isochronous cyclotrons emitting 2 ns pulses with a pulse repetition frequency of 72.8 MHz (i.e., a period of 13.7 ns)[40] would produce the least $OH^{\bullet}$ and H_2O_2 in a FLASH radiotherapy treatment.

4. Discussion

Several simplifications were introduced in this study to keep the model focused on the mechanistic effects of time structure on ROS production. A mono-energetic proton beam was used because the subsequent interaction with water leads to energy straggling that dominates over the small upstream energy spread of clinical beams. This makes the mono-energetic assumption appropriate for isolating depth-dependent energy loss and for studying the radiation chemistry stage, while a realistic clinical beam can be viewed as a superposition of many such mono-energetic components. The chemical stage was simulated in a 1.6-µm cube of water, which is sufficiently small that significant oxygen gradients are unlikely to form across it during the early microsecond regime. The oxygen concentration was therefore fixed for each tissue type. Although real tissues show spatially varying oxygen levels and dynamic oxygen diffusion,[41] modelling these features would require a full cellular geometry and a coupled diffusion–reaction framework. This is beyond the scope of the present mechanistic investigation, which aims to study relative trends in ROS yield under different pulse structures. Varying oxygen concentration or modelling oxygen transport would change the absolute G values but would not modify the qualitative trends reported here. These aspects would form the basis of future work aimed at more realistic biological scenarios.

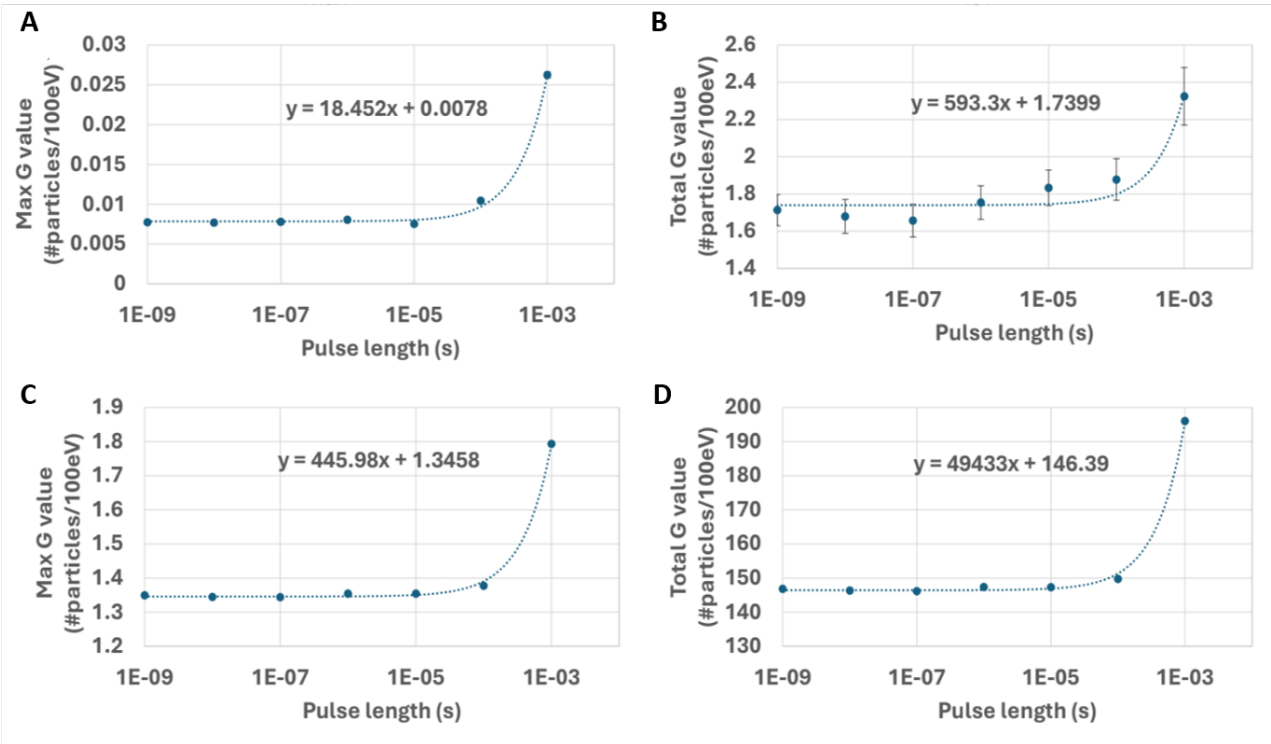

Figure 6. Plots of G_{max} and G_{tot} against pulse length for beams with long pulse lengths and short pulse periods in healthy tissue. The horizontal axis is a logarithmic scale to show the points from very short time scales to much longer time scales. (A, B) G values for $OH^{\bullet}$, and (C, D) G values for H_2O_2; (A, C) G_{max}, and (B, D) G_{tot}. All plots contain error bars; however, in (A, C, D), these are so small that they fit inside the area of the data points. Each plot also contains a linear trend line with the equation for the line.

In addition to the statistical uncertainties reported throughout this work, further uncertainty arises from the modelling assumptions themselves. These include the use of fixed oxygen concentrations, a single simulation volume, specific proton beam characteristics, model configuration, and the underlying Geant4-DNA physical and chemical interaction models. Quantifying the sensitivity of the results to each of these assumptions would require a dedicated parameter study and is beyond the scope of the present work. The results should therefore be interpreted primarily in terms of relative trends in ROS production as a function of beam pulse structure rather than as absolute quantitative predictions.

This study's main goal was to define the time-structure parameters for a proton FLASH radiotherapy beam that would lead to the fewest ROS formed in healthy tissue. This was researched under the assumption that the FLASH effect is due to oxygen depletion. In this case, the amount of ROS produced would be lower in healthy tissue for a FLASH irradiation than in a conventional irradiation, with approximately the same yield in cancer tissue. However, this is not exactly what was observed in this study: the yield of $OH^{\bullet}$ in cancer tissue was the same for FLASH and conventional exposures, but the yield in healthy tissue was higher for the FLASH dose than for the conventional dose. This appears to contradict the assumption that the FLASH effect arises from a reduction in ROS yield. However, the relationship between dose rate, radical chemistry, and biological damage is not governed solely by the absolute concentration of $OH^{\bullet}$ at early times. FLASH irradiations produce extreme temporal clustering of ionisation events, which increases the probability of radical–radical interactions across different tracks during the chemical stage. These interactions can convert highly reactive species into less damaging ones or shorten the lifetime of $OH^{\bullet}$ through rapid recombination, even if the instantaneous G value is higher. In addition, the biological consequences depend on the spatial distribution of radicals rather than only on their total yield. The dense spur overlap produced during FLASH may reduce the number of radicals that diffuse far enough to reach critical targets (i.e., DNA) within healthy cells. Therefore, a higher early $OH^{\bullet}$ G value does not necessarily imply more serious biological damage. These points show that the effect of time structure on radiochemistry is more complex than a simple comparison

of G values, and support the idea that multiple mechanisms (including radical–radical interactions, oxygen dynamics and spatial clustering) may contribute to the sparing of healthy tissue under FLASH irradiation.

Nevertheless, the yield of both $OH^{\bullet}$ and H_2O_2 varied with the time structure, with the lowest yields being achieved for short pulse periods and long pulse lengths. This qualitative description of the ideal time structure of a FLASH radiotherapy beam was refined to give the best time structure, which also corresponds to a physical delivery method for proton FLASH radiotherapy: isochronous cyclotrons emitting 2 ns pulses with a period of 13.7 ns.

Furthermore, this study succeeded in identifying a linear trend between the pulse length/period and the yield of both $OH^{\bullet}$ and H_2O_2. This linear trend was held for both the maximum and total G values. It has, however, only been tested for a pulse period which is 10 times as long as the pulse length. This is a logical relation between these parameters, and was used here so that the time structure could be investigated over a large range of values. Further work could include a more detailed study of the linear trend between the time structure and the yield of ROS for other relationships between the pulse length and period. Future work could also include a study of the evolution of the yield of other ROS with the time structure.

Finally, this study varied only the time structure of the FLASH beam, while other parameters were kept constant. These included the average dose rate, the total dose, and the beam energy. This study did not investigate variations in dose rate or total dose, even though several reports suggest that the FLASH effect is more pronounced at higher delivered doses. Such extensions would require a broader parameter space and a detailed modelling of dose-dependent oxygen depletion, radical accumulation, and longer-timescale chemistry, which lies beyond the scope of this mechanistic work. Here, the aim was to isolate the influence of the temporal beam structure on the early radiation chemistry stage under conditions that meet the accepted FLASH dose-rate threshold (40 Gy/s). Once this threshold is satisfied, the trends in ROS production associated with changes in pulse length and period can be examined without the confounding effects of dose escalation. Although different total doses may alter the absolute G values, the relative behaviour observed for varying time structures is unlikely to change, because the radical kinetics in the first microseconds scale with local track density rather than with accumulated dose. A more exhaustive study of dose-rate dependence and high-dose regimes would therefore form a natural extension of this work, especially for exploring scenarios that better reflect *in vivo* conditions.

5. Conclusion

Overall, this study identified trends in the beam time structure associated with reduced ROS yields in the specific model investigated. The conclusions should therefore be interpreted as evidence for mechanistic trends rather than as definitive predictions for clinical proton FLASH treatments. Based on the data reported, the ideal accelerator for a FLASH proton beam is an isochronous cyclotron emitting 2 ns pulses with a period of 13.7 ns. Furthermore, a linear trend was found between the time structure and the yield of ROS such as $OH^{\bullet}$ and H_2O_2.

While this research was carried out under the assumption that the FLASH effect is due to oxygen depletion, the results presented here suggest that this is not the only mechanism underpinning the sparing of healthy tissue. In fact, the results presented here seem to contradict the oxygen depletion hypothesis, as the ROS yield in healthy tissue is higher for a FLASH exposure than in the conventional case. Other factors could be at play, such as the clustering of ionisation events and radical–radical interactions, meaning that the G value is not an absolute measure of the toxicity to cells. This result would require further work to determine how the yield under FLASH irradiation evolves with a more complete model of cellular interactions.

Acknowledgments

The work was supported by the UK National Measurement System Programme in Life Sciences and Health, funded by the Department for Science, Innovation and Technology (DSIT). The authors also acknowledge the generous contribution of the De Lucia Foundation and recognise Dr Chiara D Lucia, whose vision and initiative were instrumental in initiating this work.

Funding

None.

Conflict of interest

Giuseppe Schettino is an Editorial Board Member of this journal, but was not in any way involved in the editorial and peer-review process conducted for this paper, directly or indirectly. The authors declare they have no competing interests.

Author contributions

Conceptualization: Giuseppe Schettino
Formal analysis: Jonathan Phillips
Investigation: Jonathan Phillips
Software: Jonathan Phillips

Supervision: Giuseppe Schettino
Writing–original draft: Jonathan Phillips
Writing–review & editing: All authors

Ethics approval and consent to participate

Not applicable.

Consent for publication

Not applicable.

Availability of data

The data that support the findings of this study are available from the corresponding author upon reasonable request.

References

1. Matuszak N, Suchorska WM, Milecki P, *et al.* FLASH radiotherapy: an emerging approach in radiation therapy. *Rep Pract Oncol Radiother*. 2022;27(2):343-351.

   doi: 10.5603/RPOR.a2022.0038

2. Espinosa-Rodríguez A, Sánchez-Parcerisa D, Ibáñez P, *et al.* Radical Production with Pulsed Beams: Understanding the Transition to FLASH. *Int J Mol Sci*. 2022;23(21):13484.

   doi: 10.3390/ijms232113484

3. Gaide O, Herrera F, Jeanneret Sozzi W, *et al.* Comparison of ultra-high versus conventional dose rate radiotherapy in a patient with cutaneous lymphoma. *Radiother Oncol*. 2022;174:87-91.

   doi: 10.1016/j.radonc.2021.12.045

4. Dilalla V, Chaput G, Williams T, Sultanem K. Radiotherapy side effects: Integrating a survivorship clinical lens to better serve patients. *Current Oncology*. 2020;27(2):107-112.

   doi: 10.3747/co.27.6233

5. Hughes JR, Parsons JL. FLASH Radiotherapy: Current Knowledge and Future Insights Using Proton-Beam Therapy. *Int J Mol Sci*. 2020;21(18):6492.

   doi: 10.3390/ijms21186492

6. Zhang Q, Gerweck LE, Cascio E, et al. Proton FLASH effects on mouse skin at different oxygen tensions. *Phys Med Biol*. 2023;68(5):055010.

   doi: 10.1088/1361-6560/acb888

7. Petusseau AF, Clark M, Bruza P, Gladstone D, Pogue BW. Intracellular Oxygen Transient Quantification in Vivo During Ultra-High Dose Rate FLASH Radiation Therapy. *Int J Radiat Oncol Biol Phys*. 2024;120(3):884-893.

   doi: 10.1016/j.ijrobp.2024.04.068

8. Li M, Zhou S, Dong G, Wang C. Emergence of FLASH-radiotherapy across the last 50 years (Review). *Oncol Lett*. 2024;28(6):602.

   doi: 10.3892/ol.2024.14735

9. Zhang J, Wu X, Qi P, Wang J. Prediction of the treatment effect of FLASH radiotherapy with synchrotron radiation from the Circular Electron-Positron Collider (CEPC). *J Synchrotron Radiat*. 2024;31(5):1189-1196.

   doi: 10.1107/S1600577524006878

10. Koch CJ, Kim MM, Wiersma RD. Radiation-Chemical Oxygen Depletion Depends on Chemical Environment and Dose Rate: Implications for the FLASH Effect. *Int J Radiat Oncol Biol Phys*. 2023;117(1):214-222.

    doi: 10.1016/j.ijrobp.2023.04.001

11. Cengel KA, Kim MM, Diffenderfer ES, Busch TM. FLASH Radiotherapy: What Can FLASH's Ultra High Dose Rate Offer to the Treatment of Patients With Sarcoma?. *Semin Radiat Oncol*. 2024;34(2):218-228.

    doi: 10.1016/j.semradonc.2024.02.001

12. Zhou G. Mechanisms underlying flash radiotherapy, a novel way to enlarge the differential responses to ionizing radiation between normal and tumor tissues. *Radiat Med Prot*. 2020;1(1):35-40.

    doi: 10.1016/j.radmp.2020.02.002

13. Ma J, Gao H, Shen X, Bai X, Tang M. A FLASH model of radiolytic oxygen depletion and reactive oxygen species for differential tumor and normal-tissue response. *medRxiv*. 2023.

    doi: 10.1101/2023.10.20.23297337

14. Sartorio C, Angiolini M, Flammini D, *et al.* Preliminary Assessment of Radiolysis for the Cooling Water System in the Rotating Target of SORGENTINA-RF. *Environments*. 2022; 9(8):106.

    doi: 10.3390/environments9080106

15. Dewey DL, Boag JW. Modification of the oxygen effect when bacteria are given large pulses of radiation. *Nature*. 1959;183(4673):1450-1451.

    doi: 10.1038/1831450a0

16. Boscolo D, Scifoni E, Durante M, Krämer M, Fuss MC. May oxygen depletion explain the FLASH effect? A chemical track structure analysis. *Radiother Oncol*. 2021;162:68-75.

    doi: 10.1016/j.radonc.2021.06.031

17. Adrian G, Konradsson E, Lempart M, Bäck S, Ceberg C, Petersson K. The FLASH effect depends on oxygen concentration. *Br J Radiol*. 2020;93(1106):20190702.

    doi: 10.1259/bjr.20190702

18. Geant4 Collaboration. *Geant4-DNA physics processes and models.* Updated January 14, 2026. Accessed March 3, 2026. https://geant4.web.cern.ch/documentation/dev/prm_html/PhysicsReferenceManual/electromagnetic/geant4_dna/dna.html

19. Incerti S, Baldacchino G, Bernal M. The Geant4-DNA project. *Int J Model Simul Sci Comput*. 2010;1(2):157-178.

doi: 10.1142/S1793962310000122

20. Incerti S, Ivanchenko A, Karamitros M. Comparison of Geant4 very low energy cross section models with experimental data in water. *Med Phys*. 2010;37(9):4692-4708.

doi: 10.1118/1.3476457

21. Bernal MA, Bordage MC, Brown JMC, *et al.* Track structure modeling in liquid water: A review of the Geant4-DNA very low energy extension of the Geant4 Monte Carlo simulation toolkit. *Phys Med*. 2015;31(8):861-874.

doi: 10.1016/j.ejmp.2015.10.087

22. Incerti S, Kyriakou I, Bernal MA, *et al.* Geant4-DNA example applications for track structure simulations in liquid water: A report from the Geant4-DNA Project. *Med Phys*. 2018;45(8):722-739.

doi: 10.1002/mp.13048

23. Chappuis F, Tran HN, Jorge PG, *et al.* Investigating ultra-high dose rate water radiolysis using the Geant4-DNA toolkit and a Geant4 model of the Oriatron eRT6 electron linac. *Sci Rep*. 2024;14(1):26707.

doi: 10.1038/s41598-024-76769-0

24. Lin B, Du H, Hao X, *et al.* The influence of beam parameters on FLASH effect. *Front Oncol*. 2025;15:1431700.

doi: 10.3389/fonc.2025.1431700

25. Ruan JL, Lee C, Wouters S, *et al.* Irradiation at Ultra-High (FLASH) Dose Rates Reduces Acute Normal Tissue Toxicity in the Mouse Gastrointestinal System. *Int J Radiat Oncol Biol Phys*. 2021;111(5):1250-1261.

doi: 10.1016/j.ijrobp.2021.08.004

26. Karsch L, Pawelke J, Brand M, *et al.* Beam pulse structure and dose rate as determinants for the flash effect observed in zebrafish embryo. *Radiother Oncol*. 2022;173:49-54.

doi: 10.1016/j.radonc.2022.05.025

27. Geant4 Collaboration. Release 11.4 beta. Updated June 26, 2025. Accessed October 11, 2025. Available from: https://geant4.web.cern.ch/news/2025-06-26-release11-4-beta

28. Geant4 Collaboration. Release 11.4. Updated December 5, 2025. Accessed June 12, 2026. https://geant4.web.cern.ch/news/2025-12-05-release11-4

29. Ramos-Méndez J, Shin WG, Karamitros M, *et al.* Independent reaction times method in Geant4-DNA: Implementation and performance. *Med Phys*. 2020;47(11):5919-5930.

doi: 10.1002/mp.14490

30. Bui A, Bekerat H, Childress L, Sankey J, Seuntjens J, Enger SA. Effects of incoming particle energy and cluster size on the G-value of hydrated electrons. *Phys Med*. 2023;107:102540.

doi: 10.1016/j.ejmp.2023.102540

31. Jagannathan L, Cuddapah S, Costa M. Oxidative stress under ambient and physiological oxygen tension in tissue culture. *Curr Pharmacol Rep*. 2016;2(2):64-72.

doi: 10.1007/s40495-016-0050-5

32. Colizzi I, Poulsen PR, Sørensen B, Meer D, Lomax AJ, Psoroulas S. Which 'dose rate' definition describes the FLASH sparing effect for scanned proton beams? A meta-analysis of skin murine data. *Radiother Oncol*. 2025;213:111206.

doi: 10.1016/j.radonc.2025.111206

33. Bourhis J, Sozzi WJ, Jorge PG, *et al.* Treatment of a first patient with FLASH-radiotherapy. *Radiother Oncol*. 2019;139:18-22.

doi: 10.1016/j.radonc.2019.06.019

34. Rezaee M, Iordachita I, Wong JW. Ultrahigh dose-rate (FLASH) x-ray irradiator for pre-clinical laboratory research. *Phys Med Biol*. 2021;66(9):095006.

doi: 10.1088/1361-6560/abf2fa

35. Gonçalves Jorge P, Geyer R, Kinj R, *et al.* Machine stability and dosimetry for ultra-high dose rate FLASH radiotherapy human clinical protocol. *J Appl Clin Med Phys*. 2025;26(6):e70102.

doi: 10.1002/acm2.70102

36. Panda D, Barik J. Flooding tolerance in rice: Focus on mechanisms and approaches. *Rice Sci.* 2021;28(1):43-57.

doi: 10.1016/j.rsci.2020.11.006

37. Tvrdá E, Benko F. Free radicals: what they are and what they do. In: *Pathology*. Elsevier; 2020:3-13.

doi: 10.1016/B978-0-12-815972-9.00001-9

38. Prior RL. Oxygen radical absorbance capacity (ORAC): New horizons in relating dietary antioxidants/bioactives and health benefits. *J Funct Foods*. 2015;18(Pt B):797-810.

doi: 10.1016/j.jff.2014.12.018

39. Geant4 Collaboration. *Physics processes.* Updated September 16, 2024. Accessed April 6, 2026. https://geant4.web.cern.ch/documentation/pipelines/master/bfad_html/ForApplicationDevelopers/TrackingAndPhysics/physicsProcess.html

40. Romano F, Bailat C, Jorge PG, Lerch MLF, Darafsheh A. Ultra-high dose rate dosimetry: Challenges and opportunities for FLASH radiation therapy. *Med Phys*. 2022;49(7):4912-4932.

doi: 10.1002/mp.15649

41. Pias SC. Pathways of Oxygen Diffusion in Cells and Tissues: Hydrophobic Channeling via Networked Lipids. *Adv Exp Med Biol*. 2020;1232:183-190.

doi: 10.1007/978-3-030-34461-0_23